IDENTIFYING TWO DISTINCT OLIVINE COMPOSITIONS IN TYRRHENA TERRA AND LIBYA MONTES, MARS. M. D. Lane[1], J. L. Bishop[2], D. Loizeau[3], D. Tirsch[4], L. L. Tornabene[5], L. Sacks[5], C. Viviano[6], J. R. C. Voigt[7] [1]Fibernetics LLC, Lititz, PA (lane@fibergyro.com), [2]Carl Sagan Center, SETI Institute, Mountain View, CA, [3]IAS, Université-Sud, Orsay, France, [4]Institute of Planetary Research, German Aerospace Center (DLR), Berlin, Germany, [5]Dept. of Earth Sciences, Institute for Earth and Space Exploration, University of Western Ontario, London, Canada, [6]Johns Hopkins University Applied Physics Lab (JHUAPL), Laurel, MD, [7]Lunar and Planetary Laboratory, University of Arizona, Tucson, AZ.

Introduction: Olivine is present across Terra Tyrrhena (TT) and in the southern rim of the Isidis basin in the Libya Montes (LM) region. Using both near-IR Compact Reconnaissance Imaging Spectrometer for Mars (CRISM) and mid-IR Thermal Emission Spectrometer (TES) data to characterize our study site (Fig. 1), the strongest olivine signatures across TT are identified in isolated crater floor deposits, while the olivine in the LM area is associated with a stratigraphic unit consistent with an airfall ash deposit [2]. Using mid-IR spectral indices developed from synthetic olivine data [3] for 13 different olivine compositions in the forsterite (Fo_{100}) to fayalite (Fo_0) solid solution series (Fig. 2), specific Mg-Fe olivine compositions were determined for this study area of Mars. Crater-floor olivine located across TT was determined to be Fo_{50} and the LM olivine is Fo_{65}.

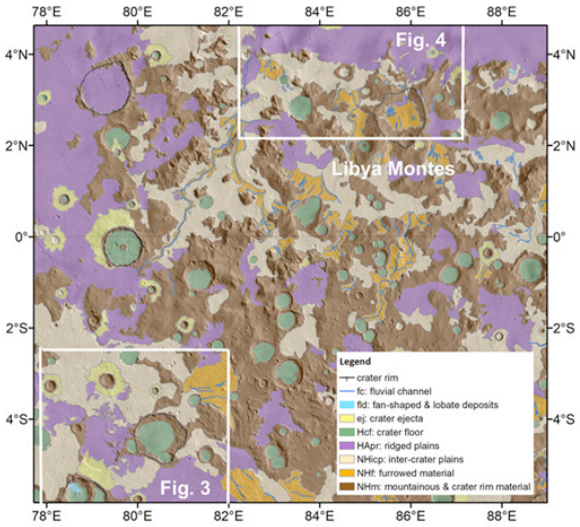

Figure 1. Geomorphologic map of the NE part of the study region (subset of map in [1]). White boxes outline the two olivine locations shown in Figs. 3 and 4.

Olivine compositions were determined utilizing data from TES (5.8 to 50 μm). This study of the TT and LM area olivine is part of a larger project [e.g., 1, 5-8] for which we are coordinating many different data sets including CRISM, HRSC, HiRISE, CTX, CaSSIS, THEMIS, and TES to interpret the regional geology and mineralogy.

TES Olivine Spectral Index: Olivine spectral indices were developed for each of 13 synthetic olivine pressed powders. These indices map a spectral feature that shifts with composition (i.e., the flection position indicated by the dot in Fig. 2 and the bands on each side). Lane and Christensen [4] successfully applied these olivine indices to TES data using JMARS software [9] by degrading the lab spectra (at 2 cm^{-1} spectral resolution) to the ~10 cm^{-1} spectral resolution of TES to correctly assign TES bands for the index formulae. These olivine indices were applied successfully to orbital TES data of the basaltic Bagnold dunes in Gale crater that contained olivine identified as $Fo_{55\ (+/-5)}$ [4]. This composition determined from orbital data subsequently was verified on the ground by the *Curiosity* rover using CheMin data that identified the dune olivine as $Fo_{56\ (+/-3)}$ [10], proving the spectral index technique to be robust.

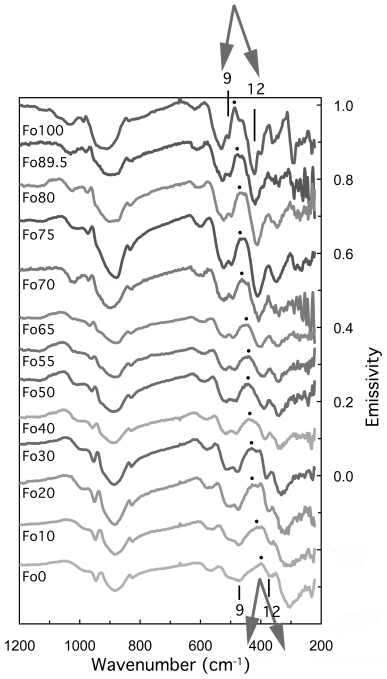

Figure 2. Thermal emissivity spectra of synthetic Mg-Fe olivines. The dots represent the flection points for each composition. These points and the bands to each side migrate with changes in chemistry. (Data from Lane et al. [3]; Figure from Lane and Christensen [4].)

TES Compositional Results: For our project's full study area (58°E to 95°E, 5°N to 26°S, c.f., [1]), TES data were used to create olivine composition index maps for the entire $Fo_{0\text{-}100}$ range. Although olivine occurs in numerous craters across TT, a good example of this crater floor composition occurs relatively close to the LM area, so we are using that smaller region as a representative example of our broader work (Fig. 1).

The best index maps were determined to be Fo_{50} and Fo_{65} for the TT craters and LM region, respectively (Figs. 3-4, top panels). The presence of olivine is further supported by higher spatial resolution mid-IR THEMIS de-correlation stretched (DCS) images (Figs. 3-4 insets in the top panels) and near-IR CRISM data [6] (Figs. 3-4 bottom panels). The mapped olivine locations correlate very well among TES, THEMIS, and CRISM data (Figs. 3-4). The yellow tones in the LM CRISM color composite suggest higher OLINDEX3 values compared to BD1300, consistent with a more Mg-rich olivine signature (Fig. 4) as compared to the TT crater floor olivine (Fig. 3).

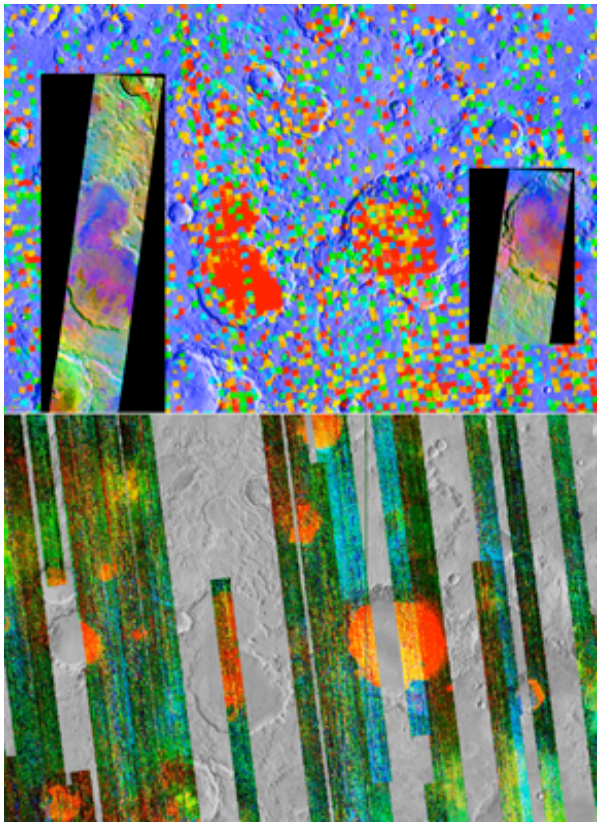

Figure 3. Top: TES Fo_{50} index map of olivine within craters (red) in the TT region. To the left and right (insets) are THEMIS DCS scenes (RGB=875) of these olivine-rich craters showing that olivine (magenta/purple) is also indicated. Bottom: CRISM mafic map (BD1300=red, olivine; OLINDEX3= green, olivine; HCPINDEX2=blue, high-Ca pyroxene).

TES spectra also match well to the lab spectra of the olivine compositions indicated by the index maps. The spectral shape of the Mars olivine was enhanced by averaging and ratioing olivine-bearing spectra to nearby olivine-deficient spectra (not shown).

Implications for Mars: Occurrences of olivine are observed using spectral data from TES, THEMIS, and CRISM in the TT to LM region. TES spectral indices for olivine demonstrated two distinct compositions, likely corresponding to different geologic events and emplacement processes. A Fo_{65} composition identified at the rim of Isidis basin corresponds mostly to interpreted airfall ash deposits [2, 8]. A Fo_{50} composition is observed for the crater-floor olivine-bearing units located across TT, which are often associated with intra-crater lava deposits (c.f., Fig. 1 and [1]).

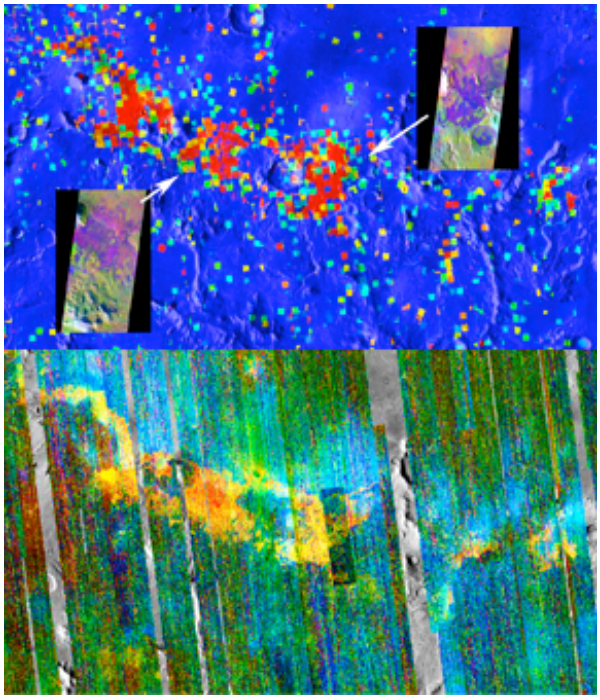

Figure 4. Top: TES Fo_{65} index map of olivine in a defined stratigraphic layer (red) at the southern rim of Isidis basin at LM. The insets are THEMIS DCS scenes (RGB=875) of two olivine-rich areas showing that olivine (magenta/purple) is also indicated. Bottom: CRISM mafic map (BD1300=red, olivine; OLINDEX3=green, olivine; HCPINDEX2=blue), high-Ca pyroxene.

Acknowledgments: This work was supported by Mars Data Analysis Program grant 80NSSC18K1384.

References: [1] Tirsch et al. (2021) 52nd LPSC, Abstract 1193. [2] Kremer et al. (2019) *Geol., 47,* 677-681. [3] Lane et al. (2011) *JGR, 116,* E08010. [4] Lane, M.D. & Christensen P.R. (2013) *GRL, 40,* 1-5. [5] Bishop et al. (2020) *Fall AGU,* Abstract P079-0008. [6] Viviano et al. (in prep.). [7] Bishop J.L., et al. (2013) *JGR, 118,* 487–513. [8] Tirsch, D., et al. (2018) *Icarus, 314,* 12-34. [9] Christensen P.R. et al. (2009) *EOS Trans. AGU., 90*(52), Fall Meet. Suppl., Abstract #IN22A-06. [10] Achilles C.N. et al. (2017) *JGR 122,* doi:10.1002/2017JE005262.